Numerical analysis of re-oscillation and non-centrosymmetric convection in a porous enclosure due to opposing heat and mass fluxes on the vertical walls

doi: 10.1016/j.icheatmasstransfer.2009.11.008

Numerical analysis of re-oscillation and non-centrosymmetric convection in a porous enclosure due to opposing heat and mass fluxes on the vertical walls

Yoshio Masuda[a*], Michio Yoneya[a], Akira Suzuki[a], Shigeo Kimura[b] and Farid Alavyoon[c]

[a] Research Center for Compact Chemical Process
National Institute of Advanced Industrial Science and Technology
4-2-1 Nigatake, Miyagino-ku, Sendai 983-8551, Japan

[b] Department of Mechanical Systems Engineering, Kanazawa University, 2-40-20 Kodatsuno, Kanazawa, Ishikawa 920-8667, Japan

[c] Forsmarks Kraftgrupp AB, SE-74203, Östhammar, Sweden

[*] Corresponding author: Tel.: +81-22-237-5211; Fax: +81-22-237-5215

E-mail address: y-masuda@aist.go.jp

ABSTRACT

Two peculiar convection patterns—re-oscillation and stable non-centrosymmetric convection—are observed when two-dimensional double-diffusive convection in a porous enclosure (aspect ratio = 1.5) is analysed numerically. The top and bottom walls of the enclosure are insulated; constant and opposing heat and mass fluxes are prescribed on the vertical walls. Re-oscillation occurs when the convection pattern changes from centrosymmetric to non-centrosymmetric. When the buoyancy ratio, which generates re-oscillation convection, is marginally lower, the convection pattern changes to stable non-centrosymmetric. These two convection patterns can be observed only for limited values of the Rayleigh number, Lewis number, and buoyancy ratio.

Keywords

Double diffusion, Porous medium, Buoyancy ratio, Numerical simulation, Peculiar convection pattern

NOMENCLATURE

A	=	aspect ratio	[-]
D	=	solute diffusivity	$[m^2 s^{-1}]$

f	=	non-dimensional frequency	[-]
g	=	acceleration due to gravity	[m s^{-2}]
2h	=	width of the enclosure	[m]
2H	=	enclosure height	[m]
k	=	permeability	[m^2]
Le	=	Lewis number	[-]
N	=	buoyancy ratio	[-]
Nu	=	Nusselt number	[-]
P	=	pressure	[-]
R	=	Rayleigh number	[-]
t	=	non-dimensional time	[-]
u	=	non-dimensional velocity vector = (u,v)	[-]
x	=	non-dimensional horizontal coordinate	[-]
y	=	non-dimensional vertical coordinate	[-]

Greek symbols

α	=	coefficient of thermal expansion	[K^{-1}]
β	=	coefficient of concentration expansion	[m^3 mol^{-1}]
ε	=	porosity	[-]
ϕ	=	non-dimensional temperature	[-]
κ	=	thermal diffusivity	[m^2 s^{-1}]
Λ_c	=	horizontal concentration gradient prescribed on the side wall	[mol m^{-4}]
Λ_T	=	horizontal temperature gradient prescribed on the side wall	[K m^{-1}]
ν	=	kinematic viscosity	[m^2 s^{-1}]
θ	=	non-dimensional concentration	[-]
σ	=	heat capacity ratio	[-]

1. INTRODUCTION

Various researchers have theoretically and numerically studied double-diffusive convection in a fluid-saturated porous enclosure due to the opposing heat and mass fluxes on the vertical walls [1-9]. In these studies, the numerical calculations yielded oscillatory solutions [7-9]. It was observed that the competition between the heat and

mass transfers with different diffusivities played an important role in generating oscillations even at low Rayleigh numbers. The convection pattern in a double-diffusive porous medium is determined by four non-dimensional parameters: the aspect ratio (A), Lewis number (Le), Rayleigh-Darcy number (R), and buoyancy ratio (N). Among the four parameters, N is expected to have the most significant effect on the characterization of the convection pattern and the oscillation, since N is the ratio of heat intensity to mass convection.

We have been investigating the double-diffusive convection in a fluid-saturated porous medium for more than 15 years. In 1994 [7], we observed oscillating convection in a double-diffusive porous medium, which, to the best of our knowledge, had not been observed before. We observed that oscillating convection occurs when R = 100; Le = 10, 20, 30, 40; and A = 3, 5, and 10. Further, we observed a monotonous oscillation pattern over one cycle. However, the characteristics of the oscillating region are not clear because the oscillating region of N was calculated at intervals of $\Delta N = 0.05$. In 2002 [8], we investigated the convection pattern only for A = 5; the oscillating region in graphs of N vs. Le for varying R were determined at intervals of $\Delta N = 0.01$. In 2007 [9], we found three peculiar types of oscillations. We discovered the re-oscillation phenomenon, which is one of the most peculiar types of oscillation. This phenomenon occurs when the convection pattern changes from centrosymmetric to non-centrosymmetric. Since this transition takes a very long time, the re-oscillation typically has a very long period. The re-oscillation phenomenon can be observed when A = 2 and 2.5. As A increases, complex oscillation can be observed more often.

In the present research, we analyse the convection patterns only when A = 1.5. If N becomes smaller than the value at which re-oscillation is observed, the Nusselt number (Nu) changes abruptly with time, and the convection pattern changes from centrosymmetric to stable (without oscillation) non-centrosymmetric, which is another peculiar convection pattern that we have observed when A = 1.5 for the first time.

In addition, we numerically study the double-diffusive convection (re-oscillation and stable non-centrosymmetric convection) in a fluid-saturated porous enclosure due to opposing heat and mass fluxes on the vertical walls. The values of R, Le, and the transition time are also investigated. One of the main objectives of the present research is to prepare an R-N map of the re-oscillation region and the stable (no oscillation)

non-centrosymmetric region.

2. PROBLEM STATEMENTS

The geometry used in the mathematical model is shown in Fig. 1. We consider a two-dimensional vertical enclosure with an aspect ratio A. This enclosure is filled with a homogeneous, fluid-saturated porous medium. The top and bottom walls of the enclosure are insulated. Constant heat flux (Λ_T) and mass flux (Λ_c) are prescribed through the vertical walls. The following equations give the momentum conservation in the Darcy regime with the Boussinesq approximation:

$$\mathbf{u} = -\nabla P - R(\theta - N\phi)\mathbf{e}_y \tag{1}$$

The equation of continuity is

$$\nabla \cdot \mathbf{u} = 0 \tag{2}$$

The equations for mass and thermal energy conservation are

$$\varepsilon \frac{\partial \theta}{\partial t} + \mathbf{u} \cdot \nabla \theta = \nabla^2 \theta \tag{3}$$

and

$$\sigma \frac{\partial \phi}{\partial t} + \mathbf{u} \cdot \nabla \phi = \mathrm{Le} \nabla^2 \phi \tag{4}$$

respectively, where $\sigma = \dfrac{\varepsilon(\rho C_p)_{liquid} + (1-\varepsilon)(\rho C_p)_{solid}}{(\rho C_p)_{liquid}}$ (5)

The boundary conditions are

$$\frac{\partial \theta}{\partial x} = -1, \frac{\partial \phi}{\partial x} = -1, \quad u = 0, \text{ and } \frac{\partial v}{\partial x} = 0 \text{ at } |x| = 1 \tag{6}$$

and $\dfrac{\partial \theta}{\partial y} = 0, \dfrac{\partial \phi}{\partial y} = 0$, $v = 0$, and $\dfrac{\partial u}{\partial y} = 0$ at $|y| = A$ (7)

The initial conditions are

$$\theta = 0, \phi = 0, \text{ and } \mathbf{u} = 0 \quad \text{at } t = 0 \tag{8}$$

The dimensionless parameters are defined as follows:

$$A = \frac{H}{h}, \quad \mathrm{Le} = \frac{\kappa}{D}, \quad R = \frac{kg\beta\Lambda_c h^2}{\nu D}, \text{ and } \quad N = \frac{\alpha\Lambda_T}{\beta\Lambda_c} \tag{9}$$

Governing equations (Eqs. 1, 2, 3, and 4) are solved numerically by the finite difference method using the boundary values (Eqs. 6 and 7) and initial conditions (Eqn.

8). The governing equations and the boundary conditions are discretised over a network of 202 × 302 grids with uniform spacing. No grid point is set on the physical boundaries (|x| = 1 and |y| = A). The first and last grid points are placed at a distance of half a grid from the boundaries. The boundary conditions at the walls are applied to these points. The numerical scheme used here is second-order accurate in space and first-order accurate in time. The matrices obtained from the governing equations are solved under the given boundary conditions by the conjugate gradient method. For further details regarding this method, please refer to Ref. [7].

In the present study, we performed calculations for the following cases: the aspect ratio A = 1.5; the Lewis number Le = 10, 20, and 30; and the non-dimensional time is less than 400. We studied the types of time-dependent Nu in this case because it is difficult to observe a drastic change the time-dependent Nu after t = 400.

3. RESULTS AND DISCUSSION

Fig. 2 shows a graph of Nu as a function of time and the flow pattern when R = 500, Le = 20, and N = 0.445. Such a pattern was referred to as the 're-oscillation case' in a previous study. The re-oscillation case is also observed when A = 1.5. Re-oscillation occurs because the convection pattern changes from non-centrosymmetric to centrosymmetric. Since this change requires a very long time, the re-oscillation typically has a very long period. For further details regarding the re-oscillation case, refer to Ref. [9]. In the case of these stream functions, positive values correspond to the clockwise flow caused by temperature gradients, while negative values correspond to the counter-clockwise flow caused by concentration gradients. The main flow represents convection due to temperature gradients, but a few convection cells due to concentration gradients can also be observed towards the left and right. The re-oscillation case is caused by convection pattern changes from non-centrosymmetric (t = 55.24) to centrosymmetric (t = 56.28). The variation of Nu with respect to time is described below. When t $\cong$ 10, the concentration diffuses in the entire domain, which brings the system to a quasi-stable steady state. However, the system starts readjusting itself to a more stable state, and this process continues up to t $\cong$ 30. Eventually, the system attains a slowly oscillating state where it is most stable. This is because such oscillations continue when t = 400.

When the value of N is marginally lower than that in the ‘re-oscillation case’, the oscillation disappears but another kind of peculiar convection can be found. Fig. 3 shows the variations in Nu and the flow pattern when R = 500, Le = 20, and N = 0.430. This figure shows that the value of Nu plummets at an early stage and attains a steady state temporally. However, Nu settles at another steady state subsequently. The convection pattern changes from centrosymmetric (t = 50) to non-centrosymmetric (t = 150). Hence, the results show that the system remains stable even when the convection pattern becomes non-centrosymmetric. Such a ‘stable non-centrosymmetric case’ is observed in the present calculation at A = 1.5, for the first time.

When N becomes considerably smaller, a centrosymmetric steady-state convection pattern can be observed. Fig. 4 has been plotted for the following values: R = 500, Le = 20, (a) N = 0.410 and (b) N = 0.400. When N = 0.40 (in Fig.4 (b)), a completely counter-clockwise convection pattern is obtained because of concentration differences. The flow speed is sluggish over the entire area when the convection due to concentration differences is the main flow. At this point, Nu becomes nearly equal to 1. On the other hand, the main convection flow is directed clockwise (Fig. 4(a)) due to temperature differences. However, the convection due to the concentration differences is dominant near the right and left side walls and the flow speed is weak, as shown in the figure. In addition, the chaotic oscillation and the ‘sudden steady state case’ observed in the former study were absent [9].

The two peculiar convection patterns, re-oscillation and stable non-centrosymmetric convection, occur because the convection pattern changes from the quasi-stable steady state to the real steady state, as shown in Figs. 2 and 3. We then investigated the relation between N and the time until Nu changes drastically. Figs. 5(a) and (b) show Nu as a function of time for three values of N during stable non-centrosymmetric convection and re-oscillation, respectively. In both cases, the transition time and the value of N are inversely proportional to each other. In our research, N is presumed to have a significant effect on the oscillation characteristics. In addition, N also has an effect on the transition time.

As the value of N reduces, convection patterns are observed in the following order: re-oscillation, stable non-centrosymmetric, temperature dominated, and concentration dominated. Fig. 6 shows the parameter range in an R-N map of the convection patterns

at (a) Le = 10, (b) Le = 20, and (c) Le = 30, at intervals of $\Delta N = 0.001$. In these three figures, the boundary line between temperature dominated and concentration dominated convections decreases monotonously as R increases. The boundary line between stable non-centrosymmetric and temperature dominated (centrosymmetric) convections also decreases monotonously as R increases, but with a comparatively smaller gradient. Therefore, the region covered by the concentration dominated convection becomes narrow as R increases. On the other hand, the region covered by the temperature dominated convection becomes wide. The region covered by the stable non-centrosymmetric convection becomes slightly wide when Le = 10; however, it remains relatively constant when Le = 20 and 30. Finally, the range of R for which the re-oscillation convection exists can be observed. For example, the R ranges from 250 to 450, 400 to 700, and 550 to 950 for Le values of 10, 20, and 30, respectively. Thus, the range of R during re-oscillation widens as Le increases. Above the re-oscillation region, various patterns can be observed; for example, oscillation continues from t = 0 to 400, or stable convection is achieved earlier. Thus, we cannot draw the parameter range in an R-N map when N is more than the region of re-oscillation.

4. CONCLUSIONS

Double diffusion in a porous enclosure has been investigated numerically for the case in which the aspect ratio of the enclosure is 1.5. The re-oscillation case, which occurs due to the convection pattern changing from centrosymmetric to non-centrosymmetric, can be observed. When the buoyancy ratio N is marginally lower than that in the re-oscillation case, the Nusselt number Nu maintains a steady state temporally and then changes to another steady state. Also, the convection pattern changes to stable non-centrosymmetric. The convection pattern is non-centrosymmetric due to temperature differences. As N becomes much smaller, a centrosymmetric convection pattern can be observed, and the pattern changes from a temperature dominated one to a concentration dominated one. Moreover, re-oscillation convection and non-centrosymmetric convection can be observed only for limited values of R, Le, and N. Because of this reason, re-oscillation convection and non-centrosymmetric convection were not discovered in previous researches. In the present study, we were able to observe these patterns clearly because we considered very small intervals of ΔN

= 0.001 and conducted the tests only when the aspect ratio of the enclosure was 1.5. Such tendency of the convection pattern change can be observed when the value of A is greater than 1.5. Further, a complex and peculiar convection can be observed when the value of A increases. On the basis of the present R-N map, we intend to develop a map with a larger aspect ratio.

REFERENCES

[1] O. Trevisan, A. Bejan, Natural convection with combined heat and mass transfer buoyancy effects in a porous medium, International Journal of Heat and Mass Transfer 28 (1985) 1597-1611.

[2] O. Trevisan, A. Bejan, Mass and heat transfer by natural convection in a vertical slot filled with porous medium, International Journal of Heat and Mass Transfer 29 (1986) 403-415.

[3] F. Alavyoon, On natural convection in vertical porous enclosures due to prescribed fluxes of heat and mass at the vertical boundaries, International Journal of Heat and Mass Transfer 36 (1993) 2479-2498.

[4] P. Bera, A. Khalili, Double-diffusive natural convection in an anisotropic porous cavity with opposing buoyancy forces: multi-solutions and oscillations, International Journal of Heat and Mass Transfer 45 (2002) 3205-3222.

[5] M. Mamou, P. Vasseur, E. Bilgen, Multiple solutions for double-diffusive convection in a vertical porous enclosure, International Journal of Heat and Mass Transfer 38 (1995) 1787-1798.

[6] A. Amahmid, M. Hasnaoui, M. Mamou, P. Vasseur, Boundary layer flows in a vertical porous enclosure induced by opposing buoyancy forces, International Journal of Heat and Mass Transfer 42 (1999) 3599-3608.

[7] F. Alavyoon, Y. Masuda, S. Kimura, On natural convection in vertical porous enclosures due to opposing fluxes of heat and mass prescribed at the vertical walls, International Journal of Heat and Mass Transfer 37 (1994) 195-206.

[8] Y. Masuda, M. Yonaya, T. Ikeshoji, S. Kimura, F. Alavyoon, T. Tsukada, M. Hozawa, Oscillatory double-diffusive convection in a porous enclosure due to opposing heat and mass fluxes on the vertical walls, International Journal of Heat and Mass Transfer 45 (2002) 1365-1369.

[9] Y. Masuda, M. Yonaya, A. Suzuki, S. Kimura, F. Alavyoon, Numerical analysis of double-diffusive convection in a porous enclosure due to opposing heat and mass fluxes on the vertical walls - Why does peculiar oscillation occur?, International Journal of Heat and Mass Transfer 51 (2008) 383-388.

Figure Captions

Fig. 1 Geometry of the porous enclosure.

Fig. 2 Nu and contour lines of stream functions for R = 500, Le = 20, and N = 0.445.

Fig. 3 Nu and contour lines of stream functions for R = 500, Le = 20, and N = 0.430.

Fig. 4 Nu and contour lines of stream functions for R = 500 and Le = 20 at (a) N = 0.410 and (b) N = 0.400.

Fig.5 Nu as a function of time for R = 500 and Le = 20 for (a) the steady non-centrosymmetric case and (b) the re-oscillation case.

Fig.6 The parameter range in an R-N map of the convection patterns at (a) Le = 10, (b) Le = 20, and (c) Le = 30.

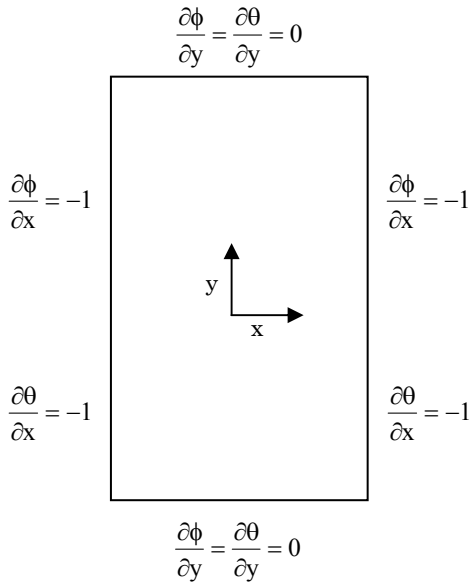
$\frac{\partial \phi}{\partial y} = \frac{\partial \theta}{\partial y} = 0$
$\frac{\partial \phi}{\partial x} = -1$
$\frac{\partial \phi}{\partial x} = -1$
y
x
$\frac{\partial \theta}{\partial x} = -1$
$\frac{\partial \theta}{\partial x} = -1$
$\frac{\partial \phi}{\partial y} = \frac{\partial \theta}{\partial y} = 0$

Fig.1

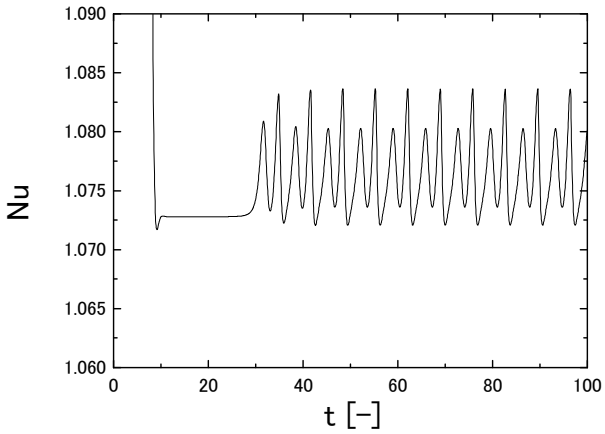

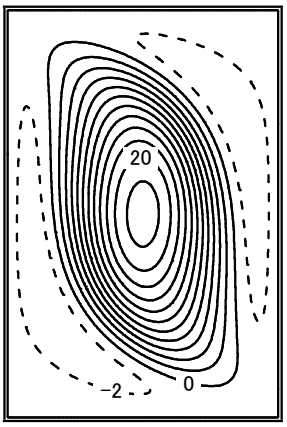

t = 20

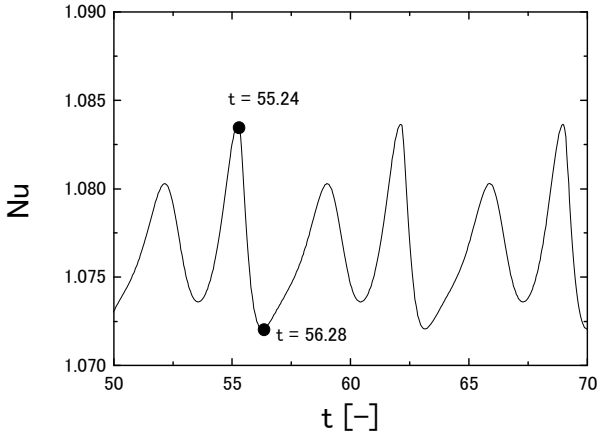

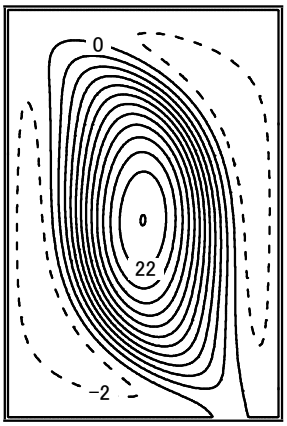

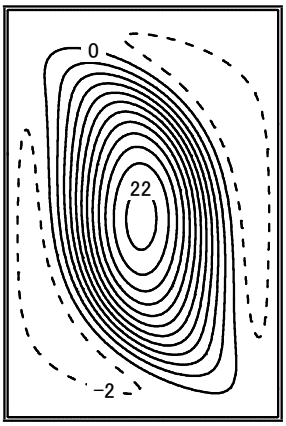

t = 55.24 t = 56.28

Fig. 2

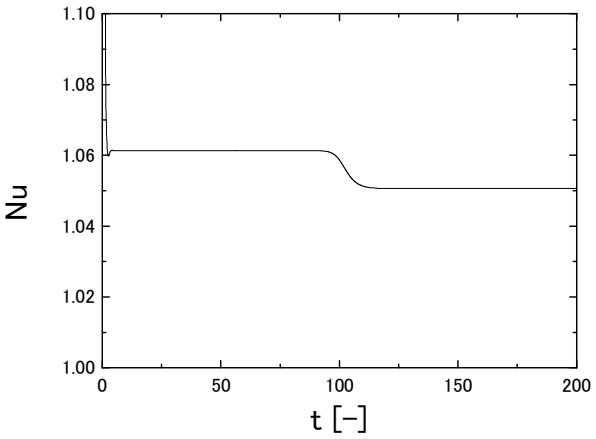

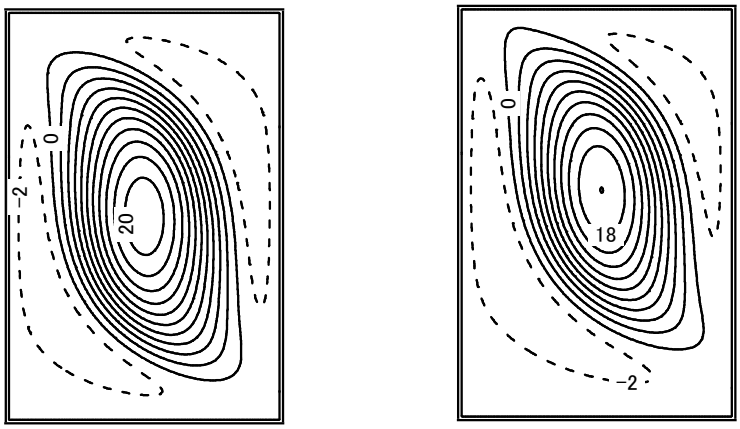

t = 50 t = 150

Fig.3

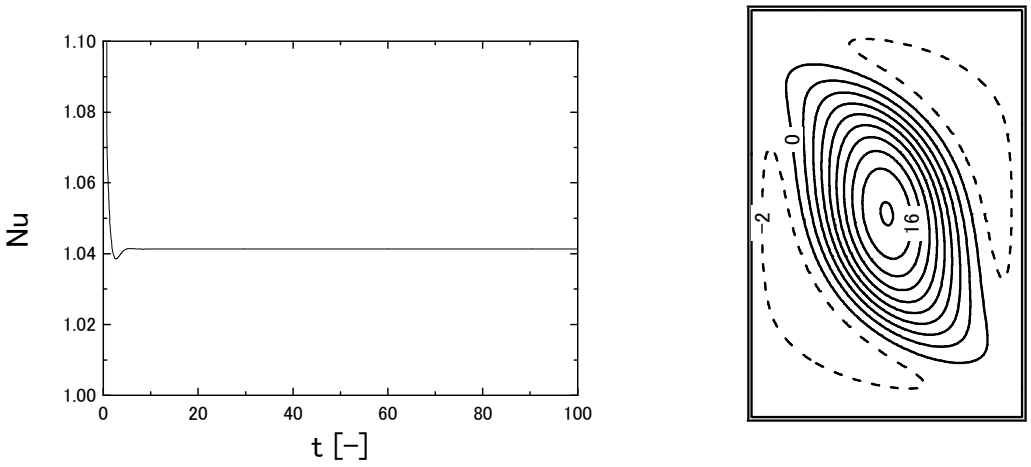

(a) N = 0.41

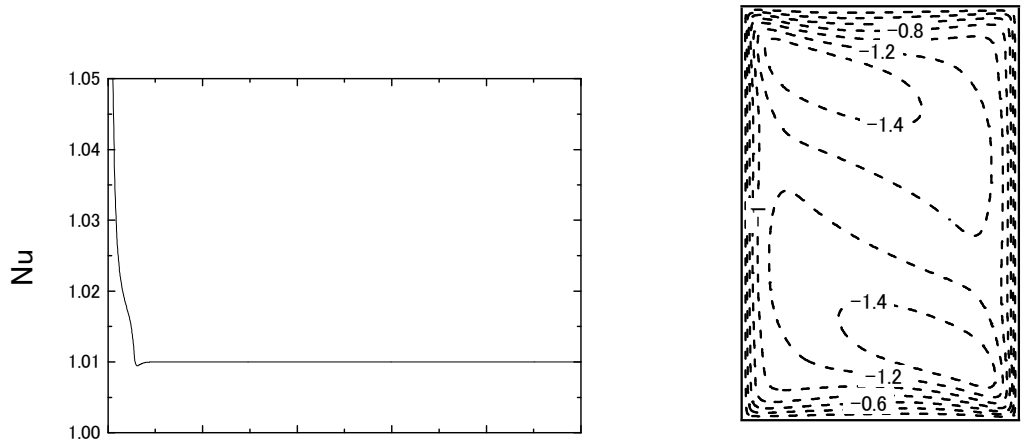

(b) N = 0.40

Fig.4

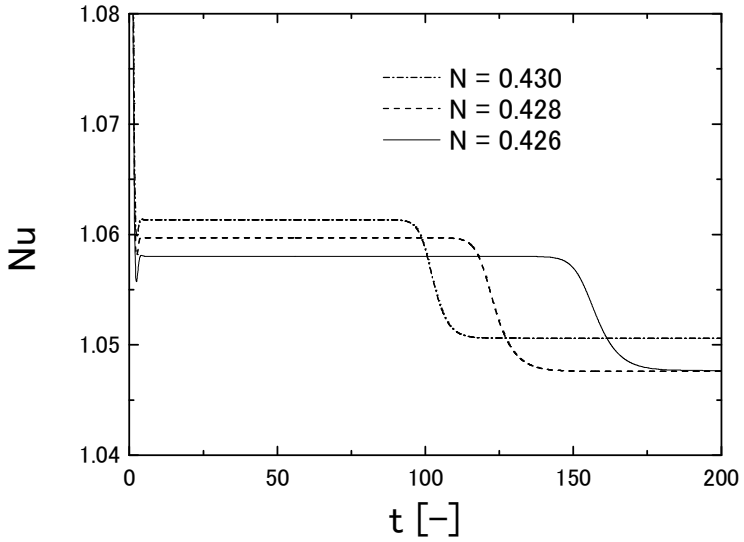
1.08
1.07
1.06
1.05
1.04
Nu
N = 0.430
N = 0.428
N = 0.426
0
50
100
150
200
t [–]

(a)

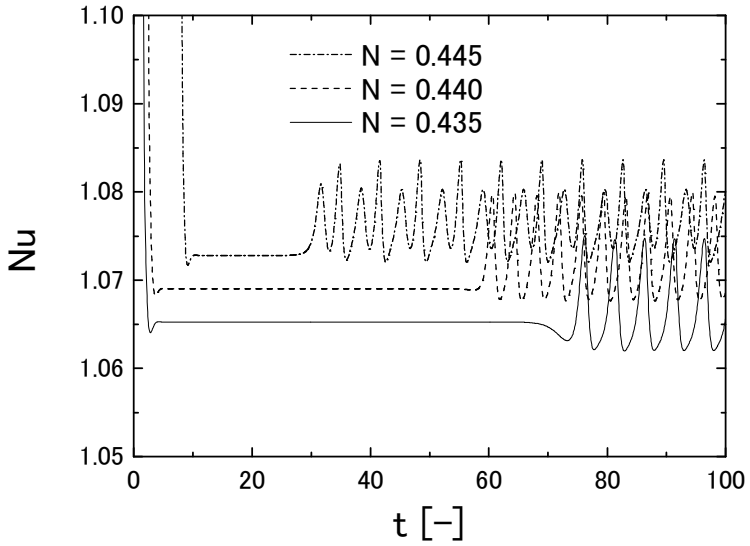
1.10
1.09
1.08
1.07
1.06
1.05
Nu
N = 0.445
N = 0.440
N = 0.435
0
20
40
60
80
100
t [–]

(b)

Fig.5

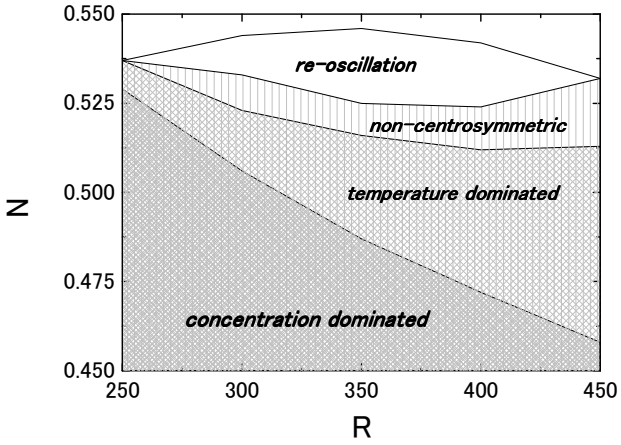

(a) Le = 10

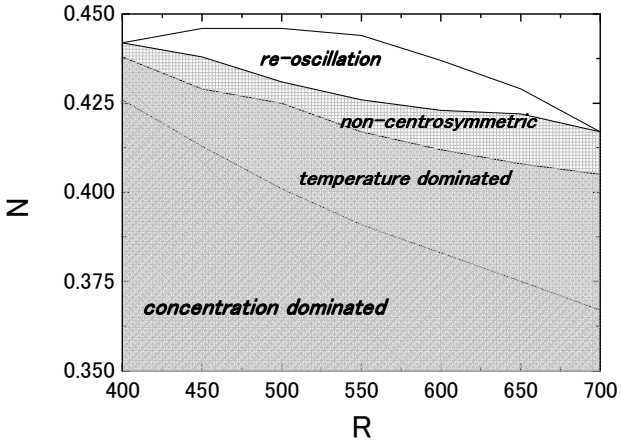

(b) Le = 20

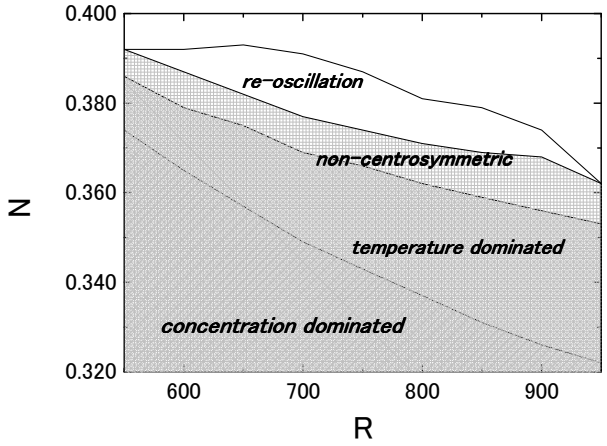

(c) Le = 30

Fig. 6